Observed Tropical Cyclone Size Revisited

DANIEL R. CHAVAS* AND NING LIN

Department of Civil and Environmental Engineering, Princeton University, Princeton, New Jersey

WENHAO DONG AND YANLUAN LIN

Ministry of Education Key Laboratory for Earth System Modeling, Center for Earth System Science, Tsinghua University, Beijing, China

(Manuscript received 14 October 2015, in final form 1 February 2016)

ABSTRACT

This work revisits the statistics of observed tropical cyclone outer size in the context of recent advances in our theoretical understanding of the storm wind field. The authors create a new dataset of the radius of 12 m s^{-1} winds based on a recently updated version of the QuikSCAT ocean wind vector database and apply an improved analytical outer wind model to estimate the outer radius of vanishing wind. The dataset is then applied to analyze the statistical distributions of the two size metrics as well as their dependence on environmental parameters, with a specific focus on testing recently identified parameters possessing credible theoretical relationships with tropical cyclone size. The ratio of the potential intensity to the Coriolis parameter is found to perform poorly in explaining variation of size, with the possible exception of its upper bound, the latter of which is in line with existing theory. The rotating radiative–convective equilibrium scaling of Khairoutdinov and Emanuel is also found to perform poorly. Meanwhile, mean storm size is found to increase systematically with the relative sea surface temperature, in quantitative agreement with the results of a recent study of storm size based on precipitation area. Implications of these results are discussed in the context of existing tropical climate theory. Finally, an empirical dependence of the central pressure deficit on outer size is found in line with past work.

1. Introduction

Though the bulk of research on tropical cyclones to date has focused on the dynamics of storm intensity, as measured by the maximum wind speed V_m, this quantity is but one component of the complete wind field, the broader understanding of which lags behind. Recent work has begun to explore the size and structure of the wind field in greater depth. In particular, Chavas et al. (2015) developed a physical model for the radial structure of the azimuthal-mean azimuthal wind that, for a given maximum wind speed and latitude, is defined relative to some absolute radial length scale that represents storm size. The model was found to compare well with observations when defining size as the radius of maximum wind r_m. Alternatively, Chavas and Lin (2016, manuscript submitted to *J. Atmos. Sci.*) demonstrate that, when defining size as the outer radius of vanishing wind r_0, the model successfully reproduces the characteristic modes of wind-field variability in nature and provides a credible prediction of r_m. As such, this model offers the potential to use outer-size information to infer inner size and structure. This outcome is significant given that r_m is the relevant size metric for damage (Zhai and Jiang 2014; Irish and Resio 2010). Additionally, r_m poses difficulties for observation because of the turbulent nature of the inner core of a tropical cyclone, including discontinuous jumps because of eyewall replacement cycles (Sitkowski et al. 2011). Moreover, in a numerical model, r_m requires high radial resolution to be credibly represented ($\leq$4 km, e.g., Chavas and Emanuel 2014), which is of particular significance in the context of climate models for which such resolutions are currently

Denotes Open Access content.

* Current affiliation: Department of Earth, Atmospheric, and Planetary Sciences, Purdue University, West Lafayette, Indiana.

Corresponding author address: Daniel R. Chavas, Department of Earth, Atmospheric, and Planetary Sciences, Purdue University, 550 Stadium Mall Drive, HAMP 3221, West Lafayette, IN 47907.
E-mail: drchavas@gmail.com

DOI: 10.1175/JCLI-D-15-0731.1

computationally expensive. In contrast, the relatively quiescent outer circulation is much more stable in time relative to the turbulent inner core, including a near independence of outer size on the maximum wind speed in both observations (Shoemaker 1989; Weatherford and Gray 1988; Merrill 1984; Chavas and Emanuel 2010; Chavas et al. 2015) and idealized numerical models (Rotunno and Bryan 2012; Chavas and Emanuel 2014). Thus, we seek to improve our understanding of outer storm size in nature, which provides a key link to our understanding of the radius of maximum wind and wind field variability in general.

How is outer storm size defined? Following the seminal work of Frank (1977), as well as more recent work by Chavas et al. (2015), the complete radial structure of a tropical cyclone may be considered to leading order to be composed of a narrow inner convecting region that varies with intensity and a broad outer nonconvecting region that does not vary with intensity, suggesting that any metric that lies sufficiently far outside of the convecting inner core may be suitable. More specifically, r_0 is fundamental to the theoretical outer wind structure model of Emanuel (2004), which has been shown to credibly reproduce the radial structure of the outer wind field in nature (Chavas et al. 2015). Unfortunately, r_0 is very difficult to estimate directly in observations or numerical models because of the combination of the decrease in data coverage and the increase in background flow variability at large radii. To avoid this issue, Chavas and Emanuel (2010) employed version 3 of the QuikSCAT global near-surface wind vector database to analyze the radius at which the azimuthal-mean azimuthal wind is $12\,\mathrm{m\,s^{-1}}$ (r_{12}), from which they estimated r_0 using the analytical outer wind model of Emanuel (2004). Alternative size metrics have also been analyzed, albeit without linkage to r_0, including the radius of $17\,\mathrm{m\,s^{-1}}$ winds from QuikSCAT (Chan and Chan 2015, 2012), the radius of $15\,\mathrm{m\,s^{-1}}$ (Shoemaker 1989; Cocks and Gray 2002), and the radius of 5-kt ($2.572\,\mathrm{m\,s^{-1}}$) winds estimated from a combination of satellite infrared data and a climatological linear model of the outer wind field (Knaff et al. 2014). All such studies have reached similar conclusions regarding the large range of variability in storm size, in line with earlier work (Merrill 1984). While all of these metrics are viable in their own right, here we focus again on r_{12}, as this metric balances the desire to maximize instrumental data coverage, to avoid the convecting inner core, and to readily separate the signal from the noise of the background flow, as originally discussed in Chavas and Emanuel (2010). Moreover, r_{12} was found to provide an optimal prediction of r_m in the complete wind structure framework of Chavas and Lin (2016, manuscript submitted to *J. Atmos. Sci.*) that links r_m and r_0. From r_{12}, we use the model of outer wind structure of Emanuel (2004), incorporating improved estimates of its input parameters, to calculate r_0.

Ultimately, the objective is an understanding of the underlying physics that governs the length scale of the outer storm circulation. Such an understanding would help explain storm size and its variation in nature, both on short time scales for operational forecasting as well as on longer time scales across climate states, including global warming. Toward this end, recent work has provided new theoretical insights into physical environmental parameters that govern this length scale. First, in rotating radiative–convective equilibrium (RCE), storm size has been demonstrated in both axisymmetric and three-dimensional geometry to scale with the ratio of the potential intensity to the Coriolis parameter V_p/f (Chavas and Emanuel 2014; Khairoutdinov and Emanuel 2013). This length scale corresponds to the intrinsic radial length scale in tropical cyclone theory [c.f. Table 1 of Emanuel (1995a)]; it also serves as a scaling for the theoretical upper bound on size [c.f. Equation 16 of Emanuel (1995b)] that arises from the need for the storm to do work to restore the angular momentum of outflow air parcels to its ambient value (Emanuel 1986). Such a scaling is consistent with the finding of Knutson et al. (2015) that global median storm size, as measured by r_{12}, remains constant under a future global warming scenario, given the anticipated increase in V_p under greenhouse warming (Emanuel 1987) as well the increase in f associated with the poleward migration of tropical cyclone activity (Kossin et al. 2014). Additionally, Chavas and Emanuel (2014) demonstrated a secondary dependence of r_0 on the nondimensional Ekman suction rate, given by $W_{\mathrm{cool}}/(C_d V_p)$, where W_{cool} is the clear-sky free-tropospheric radiative-subsidence rate and C_d is the drag coefficient that arises from Ekman balance in the outer descending region of the storm circulation. Second, Khairoutdinov and Emanuel (2013) proposed a scaling for the spacing between storms in three-dimensional rotating RCE, in which tropical cyclones fill the domain, that depends on the combination of a thermodynamic efficiency and the length scale $\sqrt{L_v q_b}/f$, where L_v is the latent heat of vaporization and q_b is the boundary layer specific humidity. This scaling was derived from global heat and energy balance constraints under the assumption that frictional dissipation by tropical cyclones dominates entropy production in the domain. Third, Lin et al. (2015) demonstrated a strong observational relationship between mean storm size, defined by the overall precipitation area, and the relative sea surface temperature (SST), defined as the difference between the local SST and its tropical mean value. Given that the relative SST in the tropics has been

shown to covary closely with local midtropospheric environmental relative humidity (Stephens 1990; Emanuel et al. 1994), this result is consistent with the prior finding of an increase in storm size with increasing environmental moisture in a numerical model (Hill and Lackmann 2009; Wang 2009). Here we investigate the extent to which each of these environmental parameters can explain variation in storm size in our observational dataset.

In addition, quantitative information on storm size variation is critical for tropical cyclone risk analysis given that r_0 is closely linked to r_m and, in turn, to storm-related hazards. Indeed, in a Monte Carlo–based storm surge risk assessment, Lin et al. (2014) showed that the surge risk could be significantly underestimated if the average storm size, as opposed to its full statistical distribution, is applied to the simulated storms. This is particularly the case when the size distribution is positively skewed, as has been observed in nature (Chavas and Emanuel 2010; Chan and Chan 2015). Moreover, in addition to potential changes in storm frequency and intensity with climate change, change of storm size can also significantly change the wind and especially surge risk (Lin et al. 2012), although storm size has been found in some model simulations to remain constant (Knutson et al. 2015) or increase marginally (Kim et al. 2014) under global warming. However, because of the limitation of current data and the lack of a rigorous understanding of the physics of storm size and its variability in the tropics, the variation of size from storm to storm and across climate states is yet to be accounted for in risk analysis (Lin and Emanuel 2016). In other applications where canonical wind–pressure relationships are used to estimate one from the other, information of storm size can also help to reduce estimation uncertainties, as the three are physically correlated.

Thus, in an effort to update and improve upon the results of Chavas and Emanuel (2010), here we first create new datasets of r_{12} and r_0 based on a recently optimized version of the QuikSCAT database and an improved version of the analytical outer wind model (section 2). Second, we analyze the variations of r_{12} and r_0 in geographic space and develop statistical distributions of each size metric globally and for each basin (section 3). Then we further investigate size variability in the context of recent advances in our understanding of storm size and structure, with a specific emphasis on testing three environmental parameters that possess credible theoretical relationships with storm size: V_p/f, the rotating RCE scaling of Khairoutdinov and Emanuel (2013), and the relative SST (section 4). Additionally, we explore empirically the effect of storm size on the canonical wind–pressure relationship (section 5). In the final section, we provide further discussion and synthesize key conclusions (section 6). This study provides new insights into storm size climatology as well as updated information for tropical cyclone risk analysis.

2. Data and methodology

a. Storm parameters

For analysis of outer storm size, we estimate the radius at which the azimuthal mean of the azimuthal wind equals $12\,\mathrm{m\,s^{-1}}$ (r_{12}) from the QuikSCAT Tropical Cyclone Radial Structure database (QSCAT-R; Chavas and Vigh 2014, available at http://verif.ral.ucar.edu/tcdata/quikscat/dataset/). QSCAT-R contains radial profiles of the azimuthal-mean azimuthal wind calculated from the NASA Jet Propulsion Laboratory (JPL) QuikSCAT tropical cyclone ocean near-surface ($z = 10\,\mathrm{m}$) wind vector database, which is a special version of version 3 of the complete global QuikSCAT dataset that has been optimized specifically for tropical cyclones using a neural network algorithm to increase accuracy and reduce rain contamination; the optimized dataset is described in Stiles et al. (2014) and is available online (http://tropicalcyclone.jpl.nasa.gov/). This global dataset spans the period 1999–2009 and has an approximate horizontal resolution of 12.5 km. A simple estimate of the near-surface background-flow vector, taken to equal the storm translation vector rotated 20° cyclonically and reduced in magnitude by a factor of 0.55 (Lin and Chavas 2012), is removed for each case prior to calculating the radial profile. Because of the common occurrence of azimuthally periodic asymmetries (Uhlhorn et al. 2014; Reasor et al. 2000), azimuthal data coverage asymmetry is a principal source of uncertainty in azimuthal-mean radial profile estimation. To quantify this uncertainty, QSCAT-R includes a data coverage asymmetry parameter ξ representing the azimuthal coverage of data at a given radius and whose value spans the range [0, 1]; a smaller value of ξ implies lower uncertainty such that $\xi = 0$ for data coverage with perfect azimuthal symmetry and $\xi = 1$ in the case of a single data point. Following the work of Chavas et al. (2015), we keep only those values of r_{12} for which $\xi \leq 0.5$ at r_{12}, and values of $r_{12} < 50\,\mathrm{km}$ (i.e., 4 times the horizontal grid spacing of the raw dataset) are ignored because of increasing uncertainty in the decomposition of flow direction at small radii. We include only cases where the storm center is over water where valid SST and potential intensity values can be estimated. In addition to wind data, QSCAT-R also includes collocated radial profiles of a quantity proportional to rain rate (denoted P^*; not accurate for absolute rain rates), based on data calculated from brightness temperature measurements taken by the SeaWinds radiometer aboard the QuikSCAT satellite (Ahmad et al. 2005). Complete details are provided in Chavas and Vigh (2014).

From r_{12}, we estimate the outer radius of vanishing azimuthal-mean azimuthal wind r_0 using the analytical model for the radial structure of the azimuthal-mean azimuthal wind in the outer, nonconvecting region first described in Emanuel (2004). This model was demonstrated to compare very well to observations by Chavas et al. (2015) and to idealized modeling simulations by Reed and Chavas (2015). The model is given by

$$\frac{\partial M}{\partial r} = \frac{2C_d}{W_{\text{cool}}} \frac{(rV)^2}{r_0^2 - r^2}, \tag{1}$$

where C_d is the surface drag coefficient, W_{cool} is the magnitude of the radiative-subsidence rate in the free troposphere, and M is the absolute angular momentum, per unit mass, given by

$$M = rV + \frac{1}{2} fr^2, \tag{2}$$

where r is the radius, V is the azimuthal wind speed, and f is the Coriolis parameter. Following Chavas et al. (2015), we specify C_d to be a function of wind speed fit to the data of Donelan et al. (2004) and the radiative-subsidence rate equal to its estimated background value of $W_{\text{cool}} = 2\,\text{mm}\,\text{s}^{-1}$, and we solve for r_0 using a shooting method. Note that, though W_{cool} is expected on theoretical grounds to remain relatively constant in space given weak temperature gradient considerations (Sobel and Bretherton 2000), its true space–time variability in nature as well as a function of radius in the outer circulation remains unknown; the value used here is taken simply as a characteristic magnitude that was found in Chavas et al. (2015) to perform well in modeling the outer wind field and that aligns with values from existing numerical modeling studies (Davis 2015; Reed and Chavas 2015). The Coriolis parameter is taken as its value at the storm center. This model was also applied in Chavas and Emanuel (2010), though with a fixed value of C_d and a much larger, arbitrary value of W_{cool} that translated to a very rapid decrease in wind speed with radius. Though in principle it is preferable to estimate the outer radius using the complete wind field model of Chavas et al. (2015), which merges this outer model with the inner model of Emanuel and Rotunno (2011), rather than the outer model alone, the result is identical except for a small subset of weak storms for which r_{12} lies within the domain of the inner model; thus, we focus on the outer region model here for simplicity. Note that a nondimensional version of Eq. (1) is described in Chavas and Lin (2016, manuscript submitted to *J. Atmos. Sci.*), where it is argued that r_0 represents a fundamental measure of storm size because of its existence as a parameter in Eq. (1) itself.

Storm-center latitude and longitude position, local storm-translation vector, maximum wind speed, and minimum central pressure are also taken from QSCAT-R. These values were interpolated from the NHC hurricane database (HURDAT) and JTWC best-track data (extracted from the International Best Track Archive for Climate Stewardship database v03r05) using a piecewise cubic Hermite interpolating polynomial, a method that eliminates overshoots between data points that can occur in traditional spline interpolation. The maximum wind speed in the best-track database is an estimate of the maximum total wind speed at any point (denoted $V_{\text{max,BT}}$) (i.e., including both storm and environmental flow effects), whereas the ideal intensity metric for this work is the maximum azimuthal-mean azimuthal wind speed associated with the storm v_{max} because of its relevance to existing tropical cyclone theory. Unfortunately, calculation of this quantity directly from QuikSCAT data is problematic because of reduced precision at high wind speeds and high rain rates common to the storm inner core (Stiles et al. 2014). Instead, we employ the dataset of maximum azimuthal-mean azimuthal wind speed of Chavas et al. (2015) calculated from the HWind near-surface wind field database (Powell et al. 1998) to develop a simple method for estimating v_{max} from best-track data alone. First, following Lin and Chavas (2012), we seek to remove the near-surface environmental flow by subtracting 55% of the translation vector magnitude V_{trans} from the best-track wind speed; this yields an estimate of the maximum point wind speed associated with the storm $V'_{\text{max,BT}}$. The reduction factor is applied because the environmental flow at the surface is weaker in magnitude than the column-integrated environmental flow (i.e., the steering flow) that governs storm motion (e.g., Chan 2005). The linear relationship of Lin and Chavas (2012) is chosen for simplicity and consistency with the methodology applied to the full wind fields from the QSCAT-R and HWind-based datasets; the nonlinear relationship of Schwerdt et al. (1979), which gives a comparable reduction factor magnitude for typical translation speeds in the tropics, was also tested and yields very similar results. Second, we estimate the relationship between this maximum point wind speed and the maximum azimuthal-mean azimuthal wind speed using the HWind database. The result is shown in Fig. 1. On average, v_{max} is approximately 80% of $V'_{\text{max,BT}}$ at all intensities, with variance that decreases steadily with increasing intensity. Thus, our estimate of the maximum azimuthal-mean azimuthal wind v^*_{max} is given by

$$v^*_{\text{max}} = 0.8(V_{\text{max,BT}} - 0.55V_{\text{trans}}), \tag{3}$$

where the asterisk denotes this simple estimate of the true value. We note that the conclusions presented below are not sensitive to the use of this alternative

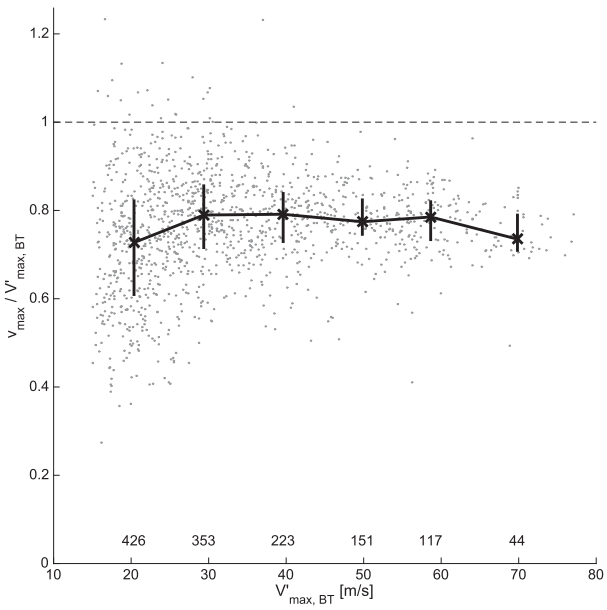

FIG. 1. Ratio of HWind azimuthal-mean azimuthal wind v_{max} to best-track intensity with translation effect removed $V'_{max,BT}$ as a function of $V'_{max,BT}$. Median (marker) and interquartile range (bar) displayed for data (dot; $N = 1314$) binned by $V'_{max,BT}$ in increments of $10\,m\,s^{-1}$ beginning at $15\,m\,s^{-1}$; final bin includes all data where $V'_{max,BT} > 65\,m\,s^{-1}$. Bin sample sizes are denoted at the bottom.

intensity metric; its use enables a more precise exploration of physical relationships among our variables of interest. For our analysis, we keep only cases for which $v^*_{max} \geq 15\,m\,s^{-1}$ ($N = 1794$). Finally, in order to place our results in the context of the commonly used Saffir–Simpson wind scale, we adjust the scale's wind speed thresholds using Eq. (3) with the translation effect fixed at $3\,m\,s^{-1}$ based on the mean translation speed of $5.38\,m\,s^{-1}$ for the dataset shown in Fig. 1. The resulting adjusted wind speed thresholds for v^*_{max} for categories 1–5 are 24.0, 32.0, 37.6, 44.8, and $53.6\,m\,s^{-1}$, respectively.

b. Environmental parameters

To calculate the length scale V_p/f, the potential intensity V_p is calculated using the standard algorithm of Bister and Emanuel (2002) with the parameter specifications of Tang and Emanuel (2012)[1] applied to the ERA-Interim monthly mean databases of SST, mean sea level pressure, temperature, and water vapor mixing ratio (Dee et al. 2011). The potential intensity is first calculated at all grid points globally for each month and then linearly interpolated in space and time to the storm-center position and day of year; monthly data are assumed to correspond to the middle of the month (e.g., 0000 UTC on day 16 for a 31-day month; leap year is ignored). The Coriolis parameter is taken as its value at the storm center.

The scaling for storm size in rotating radiative–convective equilibrium of Khairoutdinov and Emanuel (2013), given by $\sqrt{\varepsilon L_v q_b}/f$, is the product of the length scale $\sqrt{L_v q_b}/f$ and the square root of a thermodynamic efficiency, $\varepsilon = (T_s - T_0)/T_0$, where L_v is the latent heat of vaporization, q_b is the boundary layer specific humidity, T_s is the sea surface temperature, and T_0 is the inverse of the mean inverse temperature at which radiative cooling occurs in the system. The former was noted in Khairoutdinov and Emanuel (2013) to be proportional to the deformation radius in a moist adiabatic atmosphere, as the static stability, and to lesser degree the tropospheric depth, increases with increasing q_b [cf. Emanuel (1994), chapter 4; Khairoutdinov and Emanuel (2013), their Fig. 4]. Here we take q_b to be its value at 975 hPa from the ERA-Interim monthly mean database. We take T_0 to be the outflow temperature calculated from the aforementioned potential intensity algorithm, which thus defines ε to be the tropical cyclone Carnot efficiency including the effect of dissipative heating (Bister and Emanuel 1998). The velocity scale $\sqrt{\varepsilon L_v q_b}$ is interpolated in time and space in the same manner as V_p, and the Coriolis parameter is taken as its value at the storm center. Note that the prediction given by Khairoutdinov and Emanuel (2013) for the absolute value of r_0 includes a constant of proportionality given by the product of two quantities: the ratio of the radius of maximum wind to the length scale V_p/f and the ratio of r_0 to a characteristic dissipation length scale. Here we fix this constant to a value of 0.5; we do not attempt to account for variation in these quantities because they are not readily specified from available data and because we seek environmental parameters that are independent of storm-specific characteristics, such as the radius of maximum wind.

The relative SST is defined as the difference between the local SST and the tropical mean SST, the latter taken to be the mean[2] over the latitudinal band [30°S, 30°N] following the methodology of Lin et al. (2015) and past

[1] Parameter specifications: $C_k/C_d = 0.7$, pseudoadiabatic ascent, and including the effect of dissipative heating; no reduction to the $z = 10$-m level is applied, as V_p is employed here as a thermodynamic parameter and is not being compared to observed near-surface intensities. The outflow temperature T_0 is defined as the temperature at the level of neutral buoyancy of a saturated parcel lifted from the surface at the radius of maximum wind.

[2] An unweighted mean is used following Lin et al. (2015); calculation using an area-weighted mean leads to a maximum single-month difference in tropical mean SST of 0.099 K and has a negligible effect on the results.

work on the effects of remote SST on tropical cyclone activity (e.g., Vecchi and Soden 2007; Camargo et al. 2013). This quantity is calculated from the HadISST monthly SST dataset. Results are not sensitive to the precise latitudinal band employed to calculate the tropical mean SST; very similar results are obtained for [15°S, 15°N], [20°S, 20°N], and [25°S, 25°N]. Finally, for calculation of the storm central pressure deficit, the environmental sea level pressure is defined as its value interpolated to the storm time and location from monthly ERA-Interim data in the same manner as the above quantities. The use of monthly mean data acts to smooth out the contribution from the low pressure of the storm itself.

3. Size distributions

We first examine the geographic variation of storm size over the ocean basins, which is displayed in Fig. 2. Basins are defined as in Knutson et al. (2015) such that each storm's basin is assigned according to its location of genesis in the best-track database. For r_{12}, the interbasin variability in storm size in the tropics that has been identified in past work (Chavas and Emanuel 2010; Knaff et al. 2014; Chan and Chan 2015) is clearly evident. The western Pacific basin contains most of the largest storms in the dataset, though it contains some very small storms as well, indicative of both the very large storms that form from the monsoon gyre (Lander 1994) as well as the ''midget'' typhoons that occasionally form along the gyre periphery or else adjacent to the subtropical high (Arakawa 1952; Brand 1972; Lee et al. 2010). The eastern Pacific basin contains almost exclusively smaller storms. The Atlantic basin displays primarily smaller storms evident at lower latitudes in the central and eastern Atlantic, a mix of sizes at intermediate latitudes, and large sizes at high latitudes, where storms are likely transitioning to extratropical systems (Hart and Evans 2001). The north Indian Ocean basin is characterized by small and medium-sized storms, though this may simply reflect the confining coastline geometry of South Asia. In the Southern Hemisphere, both the south Indian Ocean and the South Pacific do not appear to exhibit any characteristic size.

We may compare the results between our two storm size metrics in Fig. 2, which displays the same geographic distribution for r_0 as well. In terms of size variability, the principal difference between these two quantities is the role of varying latitude: because the azimuthal wind in Eq. (1) decays more rapidly to zero for larger values of f (all else equal), the same value of r_{12} yields a smaller value of r_0 at higher latitude. Statistically, the implication of this behavior is to dampen any positive correlation between size and latitude. This effect is particularly noticeable in the Atlantic basin, where the increase in size with latitude in r_{12} largely disappears in r_0. Also, because the primary region of eastern Pacific storm activity lies at relatively low latitudes, size as measured by r_0 does not contrast as starkly with the rest of the global distribution, though it clearly remains smaller than average. Moreover, medium and large storm are more often found at relatively low latitudes in the western Pacific and thus appear even more extreme when measured by r_0. These results are qualitatively consistent with past work (Knaff et al. 2014; Chan and Chan 2015; Lee et al. 2010). More broadly, these observations highlight the complexity of examining different metrics of storm size across latitudes given the dependence of the outer wind structure on f.

Prior to further analysis, we first revisit the observed dependence of storm size on intensity. Our focus here is to study r_{12} as a metric of the size of the outer circulation, which would be expected to remain statistically steady as a function of storm intensity (Frank 1977). Figure 3 displays observed r_{12} as a function of storm intensity. We focus on the tropics and filter the data to include only cases with latitude $\phi \leq 30°$ ($N = 1538$). There is, however, a systematic increase in median size with intensity at relatively low intensities, corresponding to $v^*_{\max} \leq 32\,\mathrm{m\,s^{-1}}$. Linear regression of median r_{12} on intensity yields a best-fit slope of $7.51\,\mathrm{km\,(m\,s^{-1})^{-1}}$ {95% confidence interval (CI) = [5.5, 9.5]} over the range $v^*_{\max} \leq 32\,\mathrm{m\,s^{-1}}$. Meanwhile, median r_{12} remains nearly constant with intensity thereafter, with a linear best-fit slope that is not statistically significantly different from zero over the range $32 \leq v^*_{\max} \leq 50\,\mathrm{m\,s^{-1}}$ (95% CI = [−2.3, 3.3]). Figure 3 also displays the median QuikSCAT-estimated rain rate (proportional) at r_{12}, [denoted as $P^*(r_{12})$], as a function of intensity, which is found to systematically decrease with intensity particularly at low intensities. Linear regressions of median $P^*(r_{12})$ on intensity for the same intensity ranges as above yield a best-fit slope for low intensities that is 5.5 times larger in magnitude than at high intensities, and the latter is not statistically significantly different from zero at the 95% confidence level (not shown). In combination, this shift to stationarity is likely indicative of the transition of r_{12} consistently into the outer region, as at lower intensities r_{12} is increasingly likely to be found closer to $r_{\max}$ and thus to lie within the inner region that is sensitive to intensity. Thus, for our purposes, we consider $32\,\mathrm{m\,s^{-1}}$ to be an appropriate lower bound on intensity above which r_{12} is considered to likely lie in the outer region of the storm; this value corresponds to the threshold for category 2 in our adjusted intensity scale. Moreover, focusing on storms of at least moderate intensity is useful for risk analysis

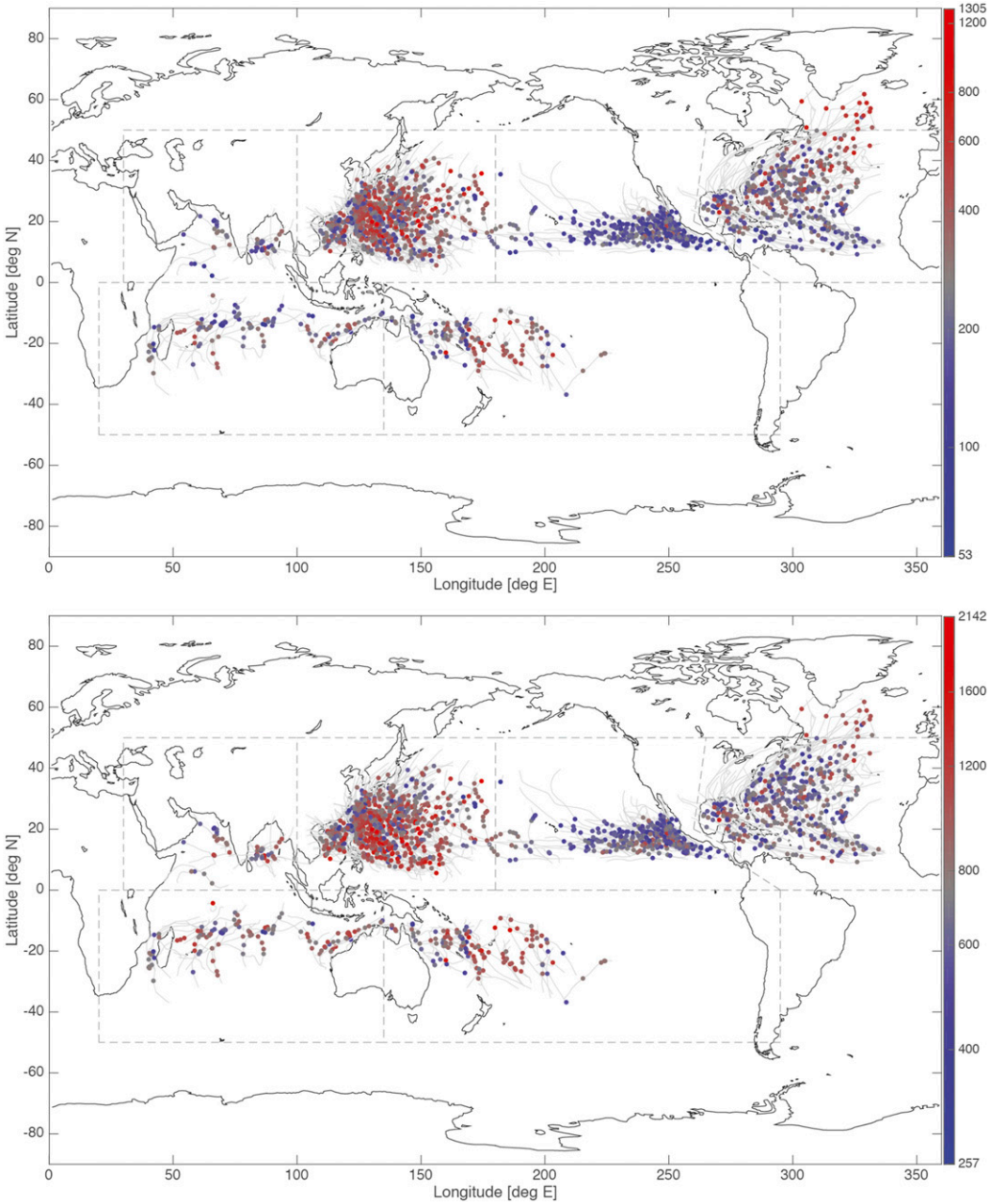

FIG. 2. Maps of spatial distribution of storm size: (top) r_{12} (km) estimated from the QSCAT-R database (1999–2009) and (bottom) r_0 (km) calculated from r_{12} using the outer region wind structure model [Eq. (1)]. Size values are shown on logarithmic scale. Gray lines denote associated storm tracks from best-track database. Dashed lines denote boundaries of basins employed in Fig. 4.

applications, as the majority of damages are caused by storms of at least category 2 intensity (Pielke Jr. et al. 2008).

Following from the results of Fig. 3, we focus our analysis on storms with intensities $v^*_{\max} \geq 32\,\mathrm{m\,s^{-1}}$ (i.e., category 2 or greater) and that are located in the tropics ($\phi \leq 30°$) to minimize potential biases introduced by extratropical interaction and rapidly translating storms typically found at higher latitudes. Figure 4 displays box-and-whisker plots of r_{12} and r_0 globally ($N = 578$) and within each ocean basin; statistics for these distributions are also provided in Table 1. The global median values of r_{12} and r_0 are 303 and 881 km with interquartile ranges of [227, 400] and [741, 1054] km, respectively. Median storm size is largest in the western Pacific and smallest in the eastern Pacific, as has been found in past work

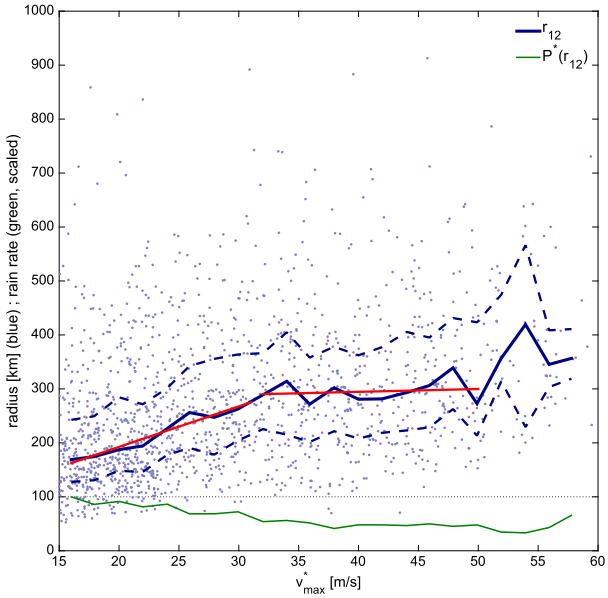

FIG. 3. Dependence of r_{12} on the estimated maximum azimuthal-mean azimuthal wind $v^*_{\max}$ Blue lines denote median (solid) and interquartile range (dashed); red lines denote linear regression on median for $v^*_{\max} \leq 32\,\mathrm{m\,s^{-1}}$ and $v^*_{\max} \in [32, 50]\,\mathrm{m\,s^{-1}}$. Green lines denote median value of quantity proportional to rain rate estimated by QuikSCAT at r_{12} (maximum value rescaled to 100). Data filtered for cases with latitude $\phi \leq 30°$ ($N = 1538$). Median values calculated in bins of $2\,\mathrm{m\,s^{-1}}$. (Two values of r_{12} exceeding 1000 km are not shown.)

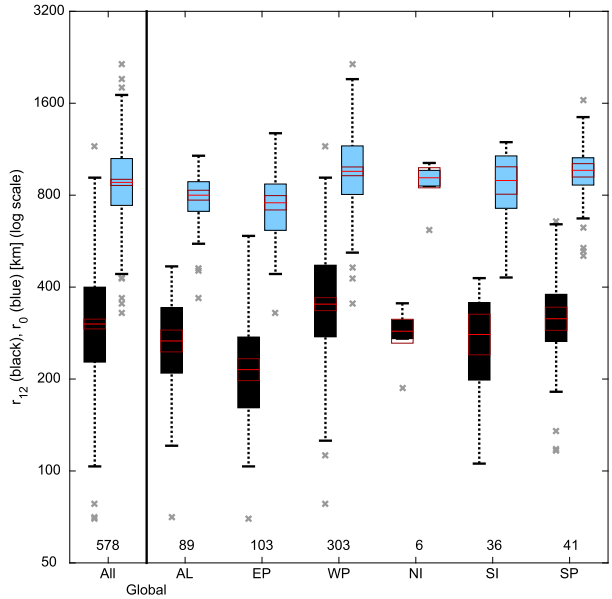

FIG. 4. Box-and-whisker plot of the distributions of r_{12} (black) and r_0 (blue) in the tropics globally and by basin. Size values are shown on logarithmic scale. Dataset filtered to include cases for which $v^*_{\max} \geq 32\,\mathrm{m\,s^{-1}}$ and latitude $\phi \leq 30°$; sample sizes are listed at the bottom. The box plot displays median (red line) and 95% confidence interval on median (dark red lines), interquartile range $[q_1, q_3]$ (black and blue fill), whiskers (black dashed lines), and outliers {gray crosses; outside the range $[q_1 - 1.5(q_3 - q_1), q_3 + 1.5(q_3 - q_1)]$ calculated from the logarithm of radius}. Corresponding statistics and basin expansions are displayed in Table 1.

(Chavas and Emanuel 2010; Knaff et al. 2014; Chan and Chan 2015); median r_0 in the South Pacific is comparable to the western Pacific. The western Pacific also exhibits the largest variance in size of any basin, though the largest coefficients of variation are found in the eastern and western Pacific basins despite their starkly contrasting mean sizes (Table 1). The global distributions of both r_{12} and r_0 are very closely lognormal, as was found in Chavas and Emanuel (2010); p values for the Kolmogorov–Smirnov (KS) goodness-of-fit test (Massey Jr. 1951) between the standardized logarithm of the data and a standard normal distribution indicate that the lognormal distribution cannot be rejected for the global distribution ($p = 0.34$) nor any of the basin distributions ($p \in [0.36, 0.93]$) at the 95% confidence level. We note that the global median value of r_{12} is approximately 50% larger than that found in Chavas and Emanuel (2010), likely because of the more rigorous filtering applied here to avoid both the low bias imposed by weaker storms and cases with higher uncertainty because of poor data coverage ξ. The values of r_0 are dramatically larger (~100%) than the prior study given the larger values of r_{12} and also the use of a proper estimate of the radiative-subsidence rate in Eq. (1), as discussed above.

TABLE 1. Statistics, including median, first and third quartiles, mean μ, standard deviation σ, and coefficient of variation, of distributions of r_{12} and r_0, corresponding to Fig. 4.

		r_{12} (km)						r_0 (km)					
Basin	N	Median	25%	75%	μ	σ	CV	Median	25%	75%	μ	σ	CV
Global	578	302.8	227.2	399.9	327.5	141.3	0.43	881.0	740.7	1054.4	909.4	248.5	0.27
North Atlantic (AL)	89	266.5	208.7	343.1	274.1	85.0	0.31	800.0	707.4	888.6	795.9	146.0	0.18
Eastern Pacific (EP)	103	214.7	160.6	279.2	235.0	101.2	0.43	755.5	613.5	870.3	759.3	189.5	0.25
Western Pacific (WP)	303	351.8	274.9	472.2	381.8	150.2	0.39	957.6	804.5	1161.0	993.5	262.7	0.26
North Indian Ocean(NI)	6	287.0	271.2	312.2	283.0	55.8	0.20	913.5	857.0	964.7	880.5	144.8	0.16
South Indian Ocean(SI)	36	279.9	198.5	356.1	275.4	92.8	0.34	893.6	724.9	1075.7	871.9	202.5	0.23
South Pacific (SP)	41	315.1	262.1	381.3	327.9	120.3	0.37	964.9	858.8	1060.5	948.1	222.1	0.23

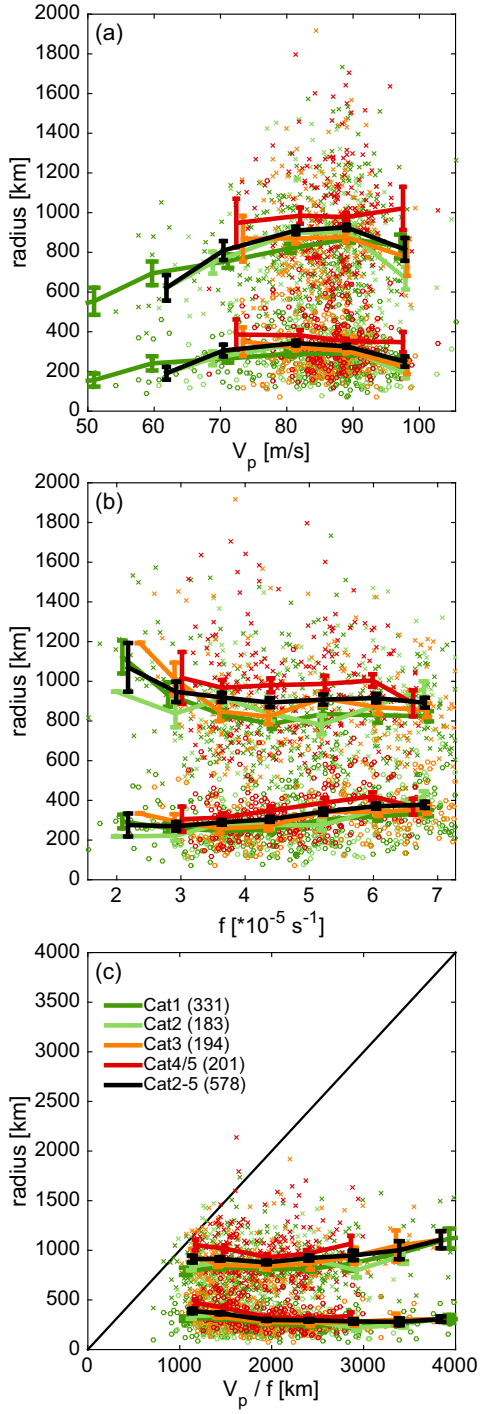

FIG. 5. Relationships between storm size and (a) V_p, (b) f, and (c) V_p/f. The bottom curves denote mean r_{12} and the top curves denote mean r_0; Circles and crosses denote all data for r_{12} and r_0, respectively. The dataset is filtered to include cases for which $\phi \leq 30°$. Results stratified by intensity according to the adjusted Saffir–Simpson category (see text for details), with sample sizes listed in the legend; the black curve denotes mean for all data with $v^*_{\max} \geq 32\,\mathrm{m\,s^{-1}}$ (i.e., categories 2–5). Error bars represent one standard error. For relationship with V_p/f, a 1:1 line is shown (black solid).

For comparison purposes, Knaff et al. (2014) estimated the wind speed at $r = 500$ km at 850 hPa, denoted V500, from which they extrapolate outward using a simple linear decay model with fixed decay rate to estimate the radius of 5-kt winds $r_{5\mathrm{kt}}$ ($1\,\mathrm{kt} \approx 0.51\,\mathrm{m\,s^{-1}}$). Absent filters for intensity or latitude, which provides the closest comparison with their methodology, the median V500 is $6.3\,\mathrm{m\,s^{-1}}$ with an interquartile range of $[4.4, 8.5]\,\mathrm{m\,s^{-1}}$ ($N = 3939$). These values are reasonably close to their estimates of 6.61 and $[5.09, 8.08]\,\mathrm{m\,s^{-1}}$, respectively; their higher values may reflect the role of friction in reducing wind speeds between 850 hPa and the surface. Furthermore, we may predict $r_{5\mathrm{kt}}$, rather than r_0, from r_{12} using Eq. (1) which yields a median value of 675 km with an interquartile range of [497, 880] km absent filters for intensity or latitude ($N = 2200$). These values are quite a bit smaller than their respective estimates of 933 and [739, 1120] km (Knaff et al. 2014). This result suggests that their linear decay model underestimates the rate of wind field decay predicted by our physical model in the outer region of the circulation, though the difference in analysis level likely contributes to this discrepancy as well.

4. Relationship to relevant environmental parameters

Ideally we seek a physical explanation of the large variability in storm size evident in Fig. 4. Thus, as a first step toward fully understanding variability in size, we test three recently identified parameters with credible physical relationships with tropical cyclone size: V_p/f, the rotating RCE scaling of Khairoutdinov and Emanuel (2013), and the relative SST. We again focus our analysis on cases from our database with $v^*_{\max} \geq 32\,\mathrm{m\,s^{-1}}$ and $\phi \leq 30°$, as was done in Fig. 4.

a. *Tropical cyclone length scale*

We begin by testing the theoretical tropical cyclone length scale V_p/f. Figure 5 displays the direct relationship between outer size and the length scale V_p/f as well as its constituent quantities. Results are stratified by intensity according to Saffir–Simpson category adjusted as described in section 2. First, there is an overall positive relationship between mean size and V_p (Fig. 5a), except at the highest values of V_p. Note that a weak positive correlation between size and V_p was identified in Chavas and Emanuel (2010), yet this relationship was dismissed arbitrarily as being too small. Here it is evident that the mean size varies systematically with V_p, even while there remains substantial residual variance about that mean value.

Though a positive relationship between size and V_p exists, no comparably strong relationship emerges

between size and f (Fig 5b). Indeed, r_{12} exhibits a slight increase with increasing f, consistent with past studies on size and latitude (Knaff et al. 2007; Mueller et al. 2006; Kossin et al. 2007). On the other hand, r_0 exhibits either no dependence or a slight decrease with increasing f for relatively small f, again an indication of how conclusions regarding the dependence of size on latitude may depend on the chosen metric. We note that there is perhaps weak evidence of a local maximum in mean r_0 at intermediate values of f, as has been found in an idealized model (Smith et al. 2011) and in observations (Chan and Chan 2015), in the vicinity of $5.5 \times 10^{-5}\,\mathrm{s}^{-1}$.

Finally, Fig. 5c displays the direct relationship between size and V_p/f. The relationship is weak, with a magnitude that is much smaller than that predicted by this length scale. However, the largest values of r_0 do appear to scale with V_p/f for values of V_p/f less than approximately 2200 km, suggesting that this length scale may indeed serve as a scaling for the upper bound on storm size, as predicted by theory in Emanuel (1986). We note that the findings of idealized equilibrium modeling studies (Khairoutdinov and Emanuel 2013; Zhou et al. 2014; Chavas and Emanuel 2014; Reed and Chavas 2015) suggest that outer storm size at equilibrium does approach this theoretical upper bound length scale. However, Fig. 5c indicates that the vast majority of storms in nature exist at sizes well below this upper bound; further discussion is provided in Section 6. Results are consistent across intensity bins and are quantitatively similar for the median in lieu of the mean. Note that we may also account for the secondary dependence of r_0 with the nondimensional Ekman suction rate, $W_{\mathrm{cool}}/(C_d V_p)$, with a scaling exponent of -0.33 found in Chavas and Emanuel (2014). Note that C_d in the outer region is not expected to vary from storm to storm, consistent with its specification in Eq. (1), while W_{cool} is expected to vary minimally in the tropics in accordance with weak temperature gradient theory (Sobel and Bretherton 2000). Thus, the result of this secondary scaling is to multiply V_p/f by an additional factor of $V_p^{0.33}$, which has little effect on the above results (not shown); this finding is not sensitive to the value of the scaling exponent.

b. *Rotating RCE scaling of Khairoutdinov and Emanuel (2013)*

We next test the rotating RCE scaling of Khairoutdinov and Emanuel (2013), given by $\sqrt{\varepsilon L_v q_b}/f$. The relationship between storm size and this scaling is shown in Fig. 6. The dependence is quite weak, similar to that of Fig. 5c. This is not surprising, given that the numerator depends on the boundary layer specific humidity, which is closely tied to the SST and hence V_p in the absence of large changes in mean SST (Ramsay and Sobel 2011). Results are quantitatively similar when keeping ε fixed as well as when replacing q_b with the saturation mixing ratio at the sea surface temperature, as was used in Khairoutdinov and Emanuel (2013).

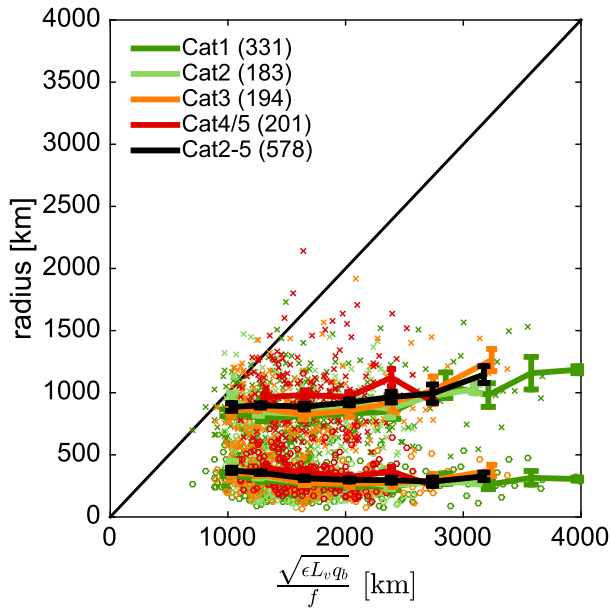

FIG. 6. As in Fig. 5c, but for the relationship between storm size and the rotating RCE scaling of Khairoutdinov and Emanuel (2013), rescaled by a constant of proportionality of 0.5 (see section 2 for details).

As noted above, the scaling of Khairoutdinov and Emanuel (2013) applies to a world in which surface frictional dissipation within tropical cyclones dominates entropy production in the system. Given that tropical cyclones typically do not cover a substantial fraction of the tropical oceans, it seems likely that the underlying assumptions of this theory may not apply in nature; indeed, the real world may lie closer to the unaggregated RCE limit in which entropy production is dominated by irreversible phase changes and diffusion of water vapor instead of frictional dissipation (Pauluis and Held 2002) and tropical cyclones impose only a weak influence on the long-term mean state. This result is also in line with the finding of Chavas and Emanuel (2014) that equilibrium storm size in an axisymmetric model does not scale with the deformation radius. Moreover, as noted in section 2, the complete theoretical prediction for r_0 also depends on the ratio of the radius of maximum wind to the length scale V_p/f and the ratio of the characteristic dissipation length scale to r_0, both of which are assumed to be constant in Khairoutdinov and Emanuel (2013). Though these assumptions may be justified in the relative homogeneity of three-dimensional rotating RCE, in which potential intensity is spatially and temporally

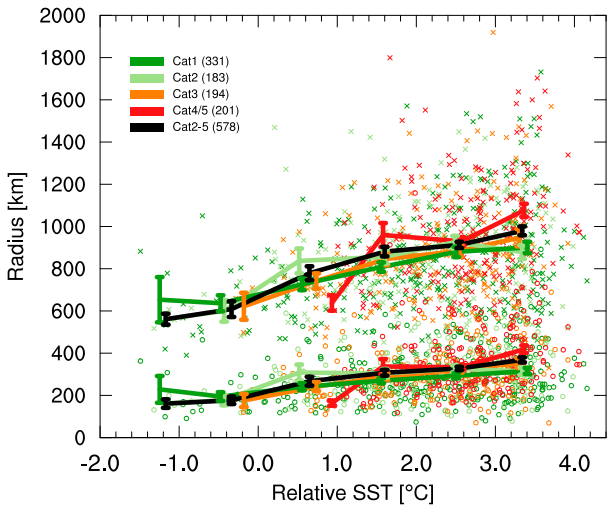

FIG. 7. As in Fig. 5a, but for the relationships between storm size and relative SST. Mean values calculated in integer bins of 1 K, with the final bin including all data above 3 K. Corresponding statistics are displayed in Table 2. Two category 1 cases with relative SST values less than −2 K are not shown.

uniform and storms are free to attain their potential intensity uninhibited, they are likely to be less valid for the real world, given its large heterogeneity.

c. *Relative SST*

Based on large samples of storm size determined from rainfall fields, Lin et al. (2015) noted a strong dependence of mean storm size on relative SST (i.e., SST within the local environment of the storm minus the tropical mean SST). Notably, relative SST correlates strongly with V_p and is often used as its surrogate (e.g., Vecchi and Soden 2007). As noted in section 1, the physical linkage of storm rainfall size with relative SST is likely manifest through its effect on midtropospheric moisture. Moreover, Lin et al. (2015) found that the precipitation-based size metric, as measured by, for example, the radius where precipitation rate equals 0.5 mm h^{-1}, is nearly insensitive to intensity, similar to the relationship found for outer wind field size as noted above. Dynamically, one expects that the wind and precipitation fields are coupled (e.g., Shoemaker 1989), and recent idealized modeling work has demonstrated that r_{12} and the radius of 1.0 mm h^{-1} rainfall are indeed highly correlated (Reed and Chavas 2015).

Thus, the logical next question is the following: Does wind field size also exhibit a dependence on relative SST? The relationship between storm size and relative SST is shown in Fig. 7. Indeed, a systematic dependence on relative SST does exist for both mean r_{12} and mean r_0; statistics are provided in Table 2. Furthermore, this dependence is consistent across intensity bins. Linear regression of mean size within each bin against mean relative SST for category 2–5 storms (i.e., the black curve in Fig. 7) gives an increase of 47.7 and 97.0 km K^{-1} for r_{12} and r_0, respectively; a similar trend is evident for category 1 storms as well. Trend magnitudes are not sensitive to the latitude band used to define the tropical-mean SST: for [25°S, 25°N], [20°S, 20°N], and [15°S, 15°N], the trend for r_{12} is 47.2, 47.1, and 43.7 km K^{-1}; and for r_0 it is 92.5, 91.9, and 84.3 km K^{-1}, respectively, where relative SST bins have been successively shifted downward by 0.5 K per 5° increment to account for the corresponding increase in mean SST. The trend for r_{12} is comparable to, though a bit larger than, the dependence of the radius of 0.5 mm h^{-1} rainfall on relative SST identified in Lin et al. (2015) of approximately 35 km K^{-1} from both TRMM data and output from an idealized numerical model simulation. This dependence of size on relative SST likely explains the dependence on its correlate V_p, shown in Fig. 5a.

Additionally, note from Table 2 that the variance increases in conjunction with the mean such that the coefficient of variation (CV) remains relatively stable across the positive relative SST bins, particularly for r_0 where the CV lies within the narrow range [0.25, 0.29]. In the negative relative SST bins, the smaller CVs are likely due to the small sample sizes: inclusion of the category 1 cases for the two lowest relative SST bins

TABLE 2. Statistics of r_{12} and r_0 binned by relative SST, corresponding to Fig. 7 for categories 2–5. Relative SST values (relSST) are the mean value within the bin.

		r_{12} (km)						r_0 (km)					
relSST (K)	N	Median	25%	75%	μ	σ	CV	Median	25%	75%	μ	σ	CV
Global	578	302.8	227.2	399.9	327.5	141.3	0.43	881.0	740.7	1054.4	909.4	248.5	0.27
−1.17	3	153.2	142.3	176.1	161.2	34.5	0.21	557.9	537.8	582.5	560.9	44.8	0.08
−0.34	8	177.0	129.6	222.3	176.9	49.8	0.28	636.3	496.0	686.3	608.6	104.9	0.17
0.65	38	238.4	180.4	318.8	267.3	128.4	0.48	750.2	674.0	878.3	778.8	201.7	0.26
1.60	129	280.9	210.3	344.1	307.3	154.5	0.50	847.3	725.2	973.8	880.9	253.5	0.29
2.54	239	305.3	245.7	396.7	327.8	124.0	0.38	897.7	763.4	1072.1	912.9	224.8	0.25
3.34	161	354.1	266.9	463.9	368.3	147.1	0.40	969.2	808.8	1140.1	979.3	264.0	0.27

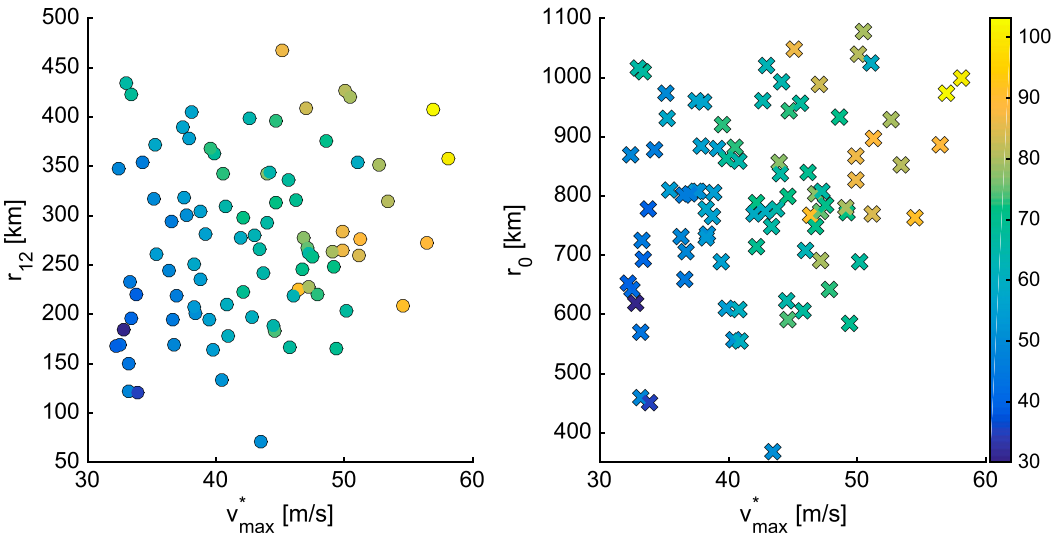

FIG. 8. Joint dependence of central pressure deficit (color, hPa) on (left) v^*_{max} and r_{12} and on (right) v^*_{max} and r_0. Data are from the Atlantic basin only for cases with $v^*_{max} \geq 32\,\mathrm{m\,s^{-1}}$ and $\phi \leq 30°$ ($N = 89$).

(-1.17 and -0.34 K) gives CVs for r_{12} of 0.43 and 0.44, respectively, and CVs for r_0 of 0.28 and 0.28, respectively, all of which align closely with their ranges for positive relative SSTs. Last, KS tests applied to the size distributions conditioned on relative SST for the bins in Table 2 indicate that the lognormal distribution cannot be rejected for any relative SST bin for both r_{12} and r_0, with all p values exceeding 0.23. Results are similar when employing the full best-track wind speed $V_{max,BT}$ as the intensity metric, as was used in Lin et al. (2015) for the rainfall field size, as well as when relative SST is calculated using data from the ERA-Interim in lieu of HadISST. Results are also similar when including data for all latitudes as well as when calculating the median in lieu of the mean. A systematic investigation of the observed relationship between the storm rainfall field and wind field will be explored in future work to corroborate previous work based on a small subset of cases (Matyas 2010).

5. Wind–pressure–size relationship

One additional relationship of interest, particularly in operations and risk analysis, is that between storm maximum wind speed and minimum central pressure: that is, the "wind–pressure" relationship. As discussed in Knaff and Zehr (2007), the storm central pressure deficit dp may be estimated from gradient wind balance as

$$dp = p_{env} - p_{min} = \int_0^{r_0} \rho \left(\frac{v^2}{r} + fv \right) dr, \qquad (4)$$

where p_{min} and p_{env} are the sea level pressures at the storm center and in the ambient environment, respectively, ρ is air density, r is radius, and v is the azimuthal component of the wind. Thus, dp depends on f and the complete radial wind profile, which may be interpreted as a wind structure defined relative to the maximum wind speed v_{max} and some absolute length scale [i.e., size (Chavas et al. 2015)]. Indeed, recent observational examples of anomalously large storms, such as Hurricane Rita (2005), illustrate how large storms can have very low central pressures despite relatively modest maximum wind speeds (Stewart 2014). More generally, past observational studies have identified a dependence of central pressure or pressure deficit on various metrics of outer storm size (Knaff and Zehr 2007; Courtney and Knaff 2009; Shoemaker 1989; Cocks and Gray 2002), as well as a role for variation in the radius of maximum wind in the context of secondary eyewall formation (Kieu et al. 2010). Moreover, in an idealized setting, Reed and Chavas (2015) demonstrated in rotating RCE aquaplanet simulations at constant f that the combination of storm intensity and outer size, as measured by r_{12}, is sufficient to explain most of the variance in the central pressure for a large dataset of storms.

Thus, here we perform a simple analysis using best-track data to test empirically whether the effect of size on central pressure deficit is discernible in our new-size dataset. Figure 8 displays the joint dependence of minimum central pressure deficit on intensity and size. We focus exclusively on data from the Atlantic basin, where independent estimates of wind intensity and minimum

central pressure are most prevalent, with data filtered for cases with $v^*_{max} \geq 32\,m\,s^{-1}$ and $\phi \leq 30°$ ($N = 89$). Though the dominant mode of variance in central pressure is associated with variation in intensity as expected, a dependence on size (r_{12} or r_0) is also evident. Indeed, for the data shown in Fig. 8, a standardized linear regression of p_{min} on the covariate v^*_{max} explains 74.5% of the variance (covariate coefficient = 0.86; one standard error = ±0.054). Adding r_{12} as a linear covariate increases the explained variance to 81.4%. Regression coefficients are 0.81 (±0.047) and 0.27 (±0.047) for v^*_{max} and r_{12}, respectively, suggesting that the contribution to central pressure deficit from intensity here is threefold larger than from size. Results are similar for r_0, for which the joint model explains 79.3% of the variance with regression coefficients of 0.80 and 0.23, indicating a 3.5-fold difference in the relative contributions of the two covariates. Notably, the explained variance is a bit higher when using the best-track maximum wind speed $V_{max,BT}$ in lieu of v^*_{max}, for which a multiple linear regression model explains 86.9% and 90.8% of the variance without and with r_{12}, respectively; for the latter case, the regression coefficient is −0.89 (±0.027) for $V_{max,BT}$ and −0.20 (±0.027) for r_{12}. This latter result likely reflects the existence of cases within the dataset that lack independent estimates of $V_{max,BT}$ and p_{min}, for which a standard wind–pressure relationship would have been applied where one intensity metric is directly specified by the other.

Despite the caveats associated with the best-track dataset noted above, the dependence of minimum central pressure on storm size is discernible from the combination of the QuikSCAT and best-track datasets in line with prior work on this subject; indeed, cases for which standard wind–pressure relationships were applied would introduce a low bias in our empirical estimate of the dependence of dp on size. These results motivate a deeper theoretical exploration of the wind–pressure–size relationship and comparison with in situ observational databases of independent wind and pressure measurements, which is the subject of future work.

6. Discussion and conclusions

This work revisits the statistics of observed tropical cyclone size explored in Chavas and Emanuel (2010) using a recently updated version of the QuikSCAT satellite scatterometer-based ocean wind vector database and places the analysis in the context of recent advances in our theoretical understanding of storm size and structure. We first create new databases of the radius of $12\,m\,s^{-1}$ winds estimated from observations from the QSCAT-R database and of the outer radius of vanishing wind r_0 estimated from r_{12} using an improved analytical outer wind model. We then analyze geographic variation in size and calculate statistical distributions of each size metric globally and for each basin. Next, we explore the dependence of storm size on environmental parameters as a first step toward understanding size variability. We focus specifically on three recently identified parameters that possess credible physical relationships with tropical cyclone outer size: 1) the theoretical tropical cyclone length scale given by the ratio of the potential intensity to the Coriolis parameter, which has been shown to govern storm size in radiative–convective equilibrium; 2) the three-dimensional rotating radiative–convective equilibrium scaling of Khairoutdinov and Emanuel (2013); and 3) the sea surface temperature relative to the tropical mean, which was shown in a recent study to govern the size of the tropical cyclone precipitation area and whose connection with storm size may be indirect via its modulation of environmental moisture. Finally, we test the relationship between storm central-pressure deficit, intensity, and size identified in past research.

We find that both metrics of outer storm size are approximately lognormally distributed, with global median values of 303 km for r_{12} and 881 km for r_0 and basin median values ranging from 215 to 352 km for r_{12} and from 756 to 965 km for r_0. The largest and smallest values are found in the western Pacific and eastern Pacific Ocean basins, respectively, corroborating the results of recent studies; the South Pacific basin was found to have a median r_0 comparable to its value in the western Pacific basin. Regarding environmental dependence, we find that variation in storm size is not well explained by the theoretical length scale V_p/f, though the absolute upper bound on size may be, in line with existing tropical cyclone theory; results are similar when accounting for a secondary dependence on the nondimensional Ekman suction rate in the outer circulation. Size variation is also found to be poorly explained by the scaling for a three-dimensional rotating RCE world, likely an indication that its underlying assumptions may not be applicable in the real world. Closer analysis of the relationship V_p/f reveals that mean storm size varies systematically with V_p but not f. This result suggests that a correlate with V_p may be relevant instead. Indeed, mean storm size is shown to vary systematically with the relative SST, which typically covaries closely with V_p. The dependence of r_{12} on relative SST is approximately $48\,km\,K^{-1}$, which is comparable to, though a bit larger than, the dependence of the radius of $0.5\,mm\,h^{-1}$ rainfall identified in Lin et al. (2015). Meanwhile, the coefficient of variation is found to remain nearly stable with relative SST. These results, in combination with the experimental

evidence of Lin et al. (2015), suggest that relative SST is indeed a more relevant parameter. We emphasize that this does not necessarily imply that V_p/f is only relevant to the upper bound of the storm size distribution, just as V_p itself is highly relevant to the dynamics of the tropical cyclone at all intensities (Tang and Emanuel 2010) despite its strict definition as the upper bound on intensity.

Importantly, for risk applications, the magnitude of the variation of size with relative SST found here is substantial given the close relationship between r_0 and r_m at fixed intensity and latitude (Chavas and Lin 2016, manuscript submitted to *J. Atmos. Sci.*). For example, we may test the sensitivity of r_m to the median variations of r_0 found here using the structural model of Chavas and Lin (2016, manuscript submitted to *J. Atmos. Sci.*): taking $v_{\max} = 40\,\mathrm{m\,s^{-1}}$, $\phi = 20°\mathrm{N}$, and $r_0 = 600\,\mathrm{km}$, a 50% increase in r_0, which corresponds to the approximate range in median size between relative SST values of 0 and 3 K, translates to a 73% increase in r_m. At landfall, such an increase in the radius of maximum wind would likely greatly enhance storm-related hazards, particularly storm surge. Moreover, we demonstrate empirically that the central pressure deficit, which is often required for, for example, storm surge modeling, is dependent on storm size, in line with prior work.

Our results beg the following question: Why does V_p/f not better explain storm size variation in nature? One existing hypothesis is that the equilibration time scale for storm size is very slow [$O(10)$ days], and thus perturbations from this length scale decay too slowly relative to the typical storm life cycle time scale in nature (Chavas and Emanuel 2014). Here we posit another hypothesis that follows from the proposed physical mechanism by which relative SST affects size: V_p/f is the relevant length scale in radiative–convective equilibrium, which is technically valid only globally in the tropics, yet in reality storms do not feel the global tropics but rather feel their local environment. This local environment is governed not by radiative–convective equilibrium but by the dynamics of the weak temperature gradient (WTG) approximation (Sobel and Bretherton 2000), which dictates that the moist ascending branch of thermally direct overturning circulations is found in regions of locally high SSTs [or, more precisely, boundary layer entropy (Emanuel et al. 1994)]. This mean ascent leads to a substantially moister local environment than would be found in RCE. Hence, the RCE length scale may not be appropriate, as alternative length scales associated with the local WTG environment may act to drive storm size away from the RCE solution. In this way, then, relative SST is representative of a distinct set of non-RCE processes, though it is not itself a length scale; elucidating the precise physical length scale at play is the subject of future work.

Additionally, we note that here we have sought explanations for variance in storm size based strictly on local environmental parameters. However, the inability of such parameters to explain large amounts of residual variance may also indicate an important role for storm-specific parameters. First and foremost, the potential existence of long time scales to equilibrium noted above may imply a long memory for size for a given storm, perhaps extending as far back as genesis. Indeed, the length scale of the precursor disturbance is not explored here, though it has been shown to correlate strongly with storm size at maturity in idealized modeling studies (Rotunno and Emanuel 1987) as well as in observations in the western North Pacific basin (Cocks and Gray 2002; Lee et al. 2010). Second, past work has noted a dependence of size simply on time since genesis (Kossin et al. 2007), which would suggest some internal physical process to the tropical cyclone that encourages expansion with time; the underlying physics of such behavior, however, have yet to be elucidated. Finally, an examination of the direct physical relationship between storm size and environmental moisture would be fruitful, though it is complicated by the strong time-dependent influence the overturning circulation of the storm itself imposes on the local moisture field. Such questions warrant further research.

We have focused principally on storm size within the tropics, purposefully avoiding the role of extratropical transition. The analyses of Fig. 2 appear to suggest that at middle and high latitudes, where extratropical transition is common, r_{12} expands with latitude in line with prior research, yet outer storm size r_0 may not, which is perhaps a reflection of an expansion of the wind field relative to a fixed outer radius, as was noted in Chavas and Lin (2016, manuscript submitted to *J. Atmos. Sci.*). However, our dataset is limited in this regard, particularly given the characteristically low intensities of storms at these high latitudes; a more detailed and/or idealized study is needed that focuses on storm size variability specifically in the context of extratropical transition. Moreover, it is worth noting that the resolution limitations of this observational dataset may inhibit us from accounting for extraordinarily small storms in nature; indeed, no theoretical lower bound on storm size currently exists.

Despite such limitations, the size distributions presented here are useful for risk analysis applications and as an observational benchmark for comparison with alternative observational size databases as well as output from both idealized modeling studies (e.g., Knutson et al. 2015) and operational weather forecasts. The

analyses on the environmental parameters provide a basis for developing environment- and climate-dependent models for storm size in the future. Finally, we note that the outer radius translates to the surface area occupied by a storm, and thus its dynamics may impose limits on the number of storms that can form in a limited area at a given time. Thus, the results presented here may be relevant for the statistics of tropical cyclogenesis in nature, particularly in localized regions where conditions favorable for genesis are spatially limited or where there is a tendency for multiple storms to form in close proximity to one another.

Acknowledgments. Support for this work was provided for DC and NL by the National Science Foundation under Award AGS-1331362 and EAR-1520683 and for WD and YL by the Ministry of Science and Technology of China Award 2014CB441303. All data in this analysis are publicly available upon request from the corresponding author.

REFERENCES

Ahmad, K. A., W. L. Jones, T. Kasparis, S. W. Vergara, I. S. Adams, and J. D. Park, 2005: Oceanic rain rate estimates from the QuikSCAT radiometer: A global precipitation mission pathfinder. *J. Geophys. Res.*, **110**, D11101, doi:10.1029/2004JD005560.

Arakawa, H., 1952: Mame-Taifu or midget typhoon. *Geophys. Mag.*, **23**, 463–474.

Bister, M., and K. A. Emanuel, 1998: Dissipative heating and hurricane intensity. *Meteor. Atmos. Phys.*, **65**, 233–240, doi:10.1007/BF01030791.

——, and ——, 2002: Low frequency variability of tropical cyclone potential intensity. 2. Climatology for 1982–1995. *J. Geophys. Res.*, **107**, 4621, doi:10.1029/2001JD000780.

Brand, S., 1972: Very large and very small typhoons of the western North Pacific Ocean. *J. Meteor. Soc. Japan*, **50**, 332–341.

Camargo, S. J., M. Ting, and Y. Kushnir, 2013: Influence of local and remote SST on North Atlantic tropical cyclone potential intensity. *Climate Dyn.*, **40**, 1515–1529, doi:10.1007/s00382-012-1536-4.

Chan, J. C., 2005: The physics of tropical cyclone motion. *Annu. Rev. Fluid Mech.*, **37**, 99–128, doi:10.1146/annurev.fluid.37.061903.175702.

Chan, K. T., and J. C. Chan, 2012: Size and strength of tropical cyclones as inferred from QuikSCAT data. *Mon. Wea. Rev.*, **140**, 811–824, doi:10.1175/MWR-D-10-05062.1.

——, and ——, 2015: Global climatology of tropical cyclone size as inferred from QuikSCAT data. *Int. J. Climatol.*, **35**, 4843–4848, doi:10.1002/joc.4307.

Chavas, D. R., and K. A. Emanuel, 2010: A QuikSCAT climatology of tropical cyclone size. *Geophys. Res. Lett.*, **37**, L18816, doi:10.1029/2010GL044558.

——, and ——, 2014: Equilibrium tropical cyclone size in an idealized state of axisymmetric radiative–convective equilibrium. *J. Atmos. Sci.*, **71**, 1663–1680, doi:10.1175/JAS-D-13-0155.1.

——, and J. Vigh, 2014: QSCAT-R: The QuikSCAT tropical cyclone radial structure dataset. NCAR Tech. Note TN-513+STR, 27 pp.

——, N. Lin, and K. Emanuel, 2015: A model for the complete radial structure of the tropical cyclone wind field. Part I: Comparison with observed structure. *J. Atmos. Sci.*, **72**, 3647–3662, doi:10.1175/JAS-D-15-0014.1.

Cocks, S. B., and W. M. Gray, 2002: Variability of the outer wind profiles of western North Pacific typhoons: Classifications and techniques for analysis and forecasting. *Mon. Wea. Rev.*, **130**, 1989–2005, doi:10.1175/1520-0493(2002)130<1989:VOTOWP>2.0.CO;2.

Courtney, J., and J. A. Knaff, 2009: Adapting the Knaff and Zehr wind–pressure relationship for operational use in Tropical Cyclone Warning Centres. *Aust. Meteor. Oceanogr. J.*, **58**, 167–179.

Davis, C. A., 2015: The formation of moist vortices and tropical cyclones in idealized simulations. *J. Atmos. Sci.*, **72**, 3499–3516, doi:10.1175/JAS-D-15-0027.1.

Dee, D., and Coauthors, 2011: The ERA-Interim reanalysis: Configuration and performance of the data assimilation system. *Quart. J. Roy. Meteor. Soc.*, **137**, 553–597, doi:10.1002/qj.828.

Donelan, M., B. Haus, N. Reul, W. Plant, M. Stiassnie, H. Graber, O. Brown, and E. Saltzman, 2004: On the limiting aerodynamic roughness of the ocean in very strong winds. *Geophys. Res. Lett.*, **31**, L18306, doi:10.1029/2004GL019460.

Emanuel, K. A., 1986: An air–sea interaction theory for tropical cyclones. Part I: Steady-state maintenance. *J. Atmos. Sci.*, **43**, 585–605, doi:10.1175/1520-0469(1986)043<0585:AASITF>2.0.CO;2.

——, 1987: The dependence of hurricane intensity on climate. *Nature*, **326**, 483–485, doi:10.1038/326483a0.

——, 1994: *Atmospheric Convection*. Oxford University Press, 580 pp.

——, 1995a: The behavior of a simple hurricane model using a convective scheme based on subcloud-layer entropy equilibrium. *J. Atmos. Sci.*, **52**, 3960–3968, doi:10.1175/1520-0469(1995)052<3960:TBOASH>2.0.CO;2.

——, 1995b: Sensitivity of tropical cyclones to surface exchange coefficients and a revised steady-state model incorporating eye dynamics. *J. Atmos. Sci.*, **52**, 3969–3976, doi:10.1175/1520-0469(1995)052<3969:SOTCTS>2.0.CO;2.

——, 2004: Tropical cyclone energetics and structure. *Atmospheric Turbulence and Mesoscale Meteorology*, E. Fedorovich, R. Rotunno, and B. Stevens, Eds., Cambridge University Press, 165–192.

——, and R. Rotunno, 2011: Self-stratification of tropical cyclone outflow. Part I: Implications for storm structure. *J. Atmos. Sci.*, **68**, 2236–2249, doi:10.1175/JAS-D-10-05024.1.

——, J. David Neelin, and C. S. Bretherton, 1994: On large-scale circulations in convecting atmospheres. *Quart. J. Roy. Meteor. Soc.*, **120**, 1111–1143, doi:10.1002/qj.49712051902.

Frank, W. M., 1977: The structure and energetics of the tropical cyclone. I: Storm structure. *Mon. Wea. Rev.*, **105**, 1119–1135, doi:10.1175/1520-0493(1977)105<1119:TSAEOT>2.0.CO;2.

Hart, R. E., and J. L. Evans, 2001: A climatology of the extratropical transition of Atlantic tropical cyclones. *J. Climate*, **14**, 546–564, doi:10.1175/1520-0442(2001)014<0546:ACOTET>2.0.CO;2.

Hill, K. A., and G. M. Lackmann, 2009: Influence of environmental humidity on tropical cyclone size. *Mon. Wea. Rev.*, **137**, 3294–3315, doi:10.1175/2009MWR2679.1.

Irish, J. L., and D. T. Resio, 2010: A hydrodynamics-based surge scale for hurricanes. *Ocean Eng.*, **37**, 69–81, doi:10.1016/j.oceaneng.2009.07.012.

Khairoutdinov, M., and K. Emanuel, 2013: Rotating radiative-convective equilibrium simulated by a cloud-resolving model.

J. Adv. Model. Earth Syst., **5**, 816–825, doi:10.1002/2013MS000253.

Kieu, C. Q., H. Chen, and D.-L. Zhang, 2010: An examination of the pressure–wind relationship for intense tropical cyclones. *Wea. Forecasting*, **25**, 895–907, doi:10.1175/2010WAF2222344.1.

Kim, H.-S., G. A. Vecchi, T. R. Knutson, W. G. Anderson, T. L. Delworth, A. Rosati, F. Zeng, and M. Zhao, 2014: Tropical cyclone simulation and response to CO_2 doubling in the GFDL CM2.5 high-resolution coupled climate model. *J. Climate*, **27**, 8034–8054, doi:10.1175/JCLI-D-13-00475.1.

Knaff, J. A., and R. M. Zehr, 2007: Reexamination of tropical cyclone wind–pressure relationships. *Wea. Forecasting*, **22**, 71–88, doi:10.1175/WAF965.1.

——, C. R. Sampson, M. DeMaria, T. P. Marchok, J. M. Gross, and C. J. McAdie, 2007: Statistical tropical cyclone wind radii prediction using climatology and persistence. *Wea. Forecasting*, **22**, 781–791, doi:10.1175/WAF1026.1.

——, S. P. Longmore, and D. A. Molenar, 2014: An objective satellite-based tropical cyclone size climatology. *J. Climate*, **27**, 455–476, doi:10.1175/JCLI-D-13-00096.1; Corrigendum, **28**, 8648–8651, doi:10.1175/JCLI-D-15-0610.1.

Knutson, T., J. Sirutis, M. Zhao, R. Tuleya, M. Bender, G. Vecchi, G. Villarini, and D. Chavas, 2015: Global projections of intense tropical cyclone activity for the late twenty-first century from dynamical downscaling of CMIP5/RCP4.5 scenarios. *J. Climate*, **28**, 7203–7224, doi:10.1175/JCLI-D-15-0129.1.

Kossin, J. P., J. A. Knaff, H. I. Berger, D. C. Herndon, T. A. Cram, C. S. Velden, R. J. Murnane, and J. D. Hawkins, 2007: Estimating hurricane wind structure in the absence of aircraft reconnaissance. *Wea. Forecasting*, **22**, 89–101, doi:10.1175/WAF985.1.

——, K. A. Emanuel, and G. A. Vecchi, 2014: The poleward migration of the location of tropical cyclone maximum intensity. *Nature*, **509**, 349–352, doi:10.1038/nature13278.

Lander, M. A., 1994: Description of a monsoon gyre and its effects on the tropical cyclones in the western North Pacific during August 1991. *Wea. Forecasting*, **9**, 640–654, doi:10.1175/1520-0434(1994)009<0640:DOAMGA>2.0.CO;2.

Lee, C.-S., K. K. Cheung, W.-T. Fang, and R. L. Elsberry, 2010: Initial maintenance of tropical cyclone size in the western North Pacific. *Mon. Wea. Rev.*, **138**, 3207–3223, doi:10.1175/2010MWR3023.1.

Lin, N., and D. Chavas, 2012: On hurricane parametric wind and applications in storm surge modeling. *J. Geophys. Res.*, **117**, D09120, doi:10.1029/2011JD017126.

——, and K. A. Emanuel, 2016: Grey swan tropical cyclones. *Nat. Climate Change*, **6**, 106–111, doi:10.1038/nclimate2777.

——, ——, M. Oppenheimer, and E. Vanmarcke, 2012: Physically based assessment of hurricane surge threat under climate change. *Nat. Climate Change*, **2**, 462–467, doi:10.1038/nclimate1389.

——, P. Lane, K. A. Emanuel, R. M. Sullivan, and J. P. Donnelly, 2014: Heightened hurricane surge risk in northwest Florida revealed from climatological-hydrodynamic modeling and paleorecord reconstruction. *J. Geophys. Res.*, **119**, 8606–8623, doi:10.1002/2014JD021584.

Lin, Y., M. Zhao, and M. Zhang, 2015: Tropical cyclone rainfall area controlled by relative sea surface temperature. *Nat. Commun.*, **6**, 6591, doi:10.1038/ncomms7591.

Massey, F. J., Jr., 1951: The Kolmogorov–Smirnov test for goodness of fit. *J. Amer. Stat. Assoc.*, **46**, 68–78, doi:10.1080/01621459.1951.10500769.

Matyas, C. J., 2010: Associations between the size of hurricane rain fields at landfall and their surrounding environments. *Meteor. Atmos. Phys.*, **106**, 135–148, doi:10.1007/s00703-009-0056-1.

Merrill, R. T., 1984: A comparison of large and small tropical cyclones. *Mon. Wea. Rev.*, **112**, 1408–1418, doi:10.1175/1520-0493(1984)112<1408:ACOLAS>2.0.CO;2.

Mueller, K. J., M. DeMaria, J. Knaff, J. P. Kossin, and T. H. Vonder Haar, 2006: Objective estimation of tropical cyclone wind structure from infrared satellite data. *Wea. Forecasting*, **21**, 990–1005, doi:10.1175/WAF955.1.

Pauluis, O., and I. M. Held, 2002: Entropy budget of an atmosphere in radiative–convective equilibrium. Part I: Maximum work and frictional dissipation. *J. Atmos. Sci.*, **59**, 125–139, doi:10.1175/1520-0469(2002)059<0125:EBOAAI>2.0.CO;2.

Pielke, R. A., Jr., J. Gratz, C. W. Landsea, D. Collins, M. A. Saunders, and R. Musulin, 2008: Normalized hurricane damages in the United States: 1900–2005. *Nat. Hazards Rev.*, **9**, 29–42, doi:10.1061/(ASCE)1527-6988(2008)9:1(29).

Powell, M. D., S. H. Houston, L. R. Amat, and N. Morisseau-Leroy, 1998: The HRD real-time hurricane wind analysis system. *J. Wind Eng. Ind. Aerodyn.*, **77–78**, 53–64, doi:10.1016/S0167-6105(98)00131-7.

Ramsay, H. A., and A. H. Sobel, 2011: Effects of relative and absolute sea surface temperature on tropical cyclone potential intensity using a single-column model. *J. Climate*, **24**, 183–193, doi:10.1175/2010JCLI3690.1.

Reasor, P. D., M. T. Montgomery, F. D. Marks Jr., and J. F. Gamache, 2000: Low-wavenumber structure and evolution of the hurricane inner core observed by airborne dual-doppler radar. *Mon. Wea. Rev.*, **128**, 1653–1680, doi:10.1175/1520-0493(2000)128<1653:LWSAEO>2.0.CO;2.

Reed, K. A., and D. R. Chavas, 2015: Uniformly rotating global radiative–convective equilibrium in the Community Atmosphere Model, version 5. *J. Adv. Model. Earth Syst.*, **7**, 1938–1955, doi:10.1002/2015MS000519.

Rotunno, R., and K. A. Emanuel, 1987: An air–sea interaction theory for tropical cyclones. Part II: Evolutionary study using a nonhydrostatic axisymmetric numerical model. *J. Atmos. Sci.*, **44**, 542–561, doi:10.1175/1520-0469(1987)044<0542:AAITFT>2.0.CO;2.

——, and G. H. Bryan, 2012: Effects of parameterized diffusion on simulated hurricanes. *J. Atmos. Sci.*, **69**, 2284–2299, doi:10.1175/JAS-D-11-0204.1.

Schwerdt, R. W., F. P. Ho, and R. R. Watkins, 1979: Meteorological criteria for standard project hurricane and probable maximum hurricane windfields, Gulf and East Coasts of the United States. NOAA Tech. Rep. NWS 23, 317 pp.

Shoemaker, D. N., 1989: Relationships between tropical cyclone deep convection and the radial extent of damaging winds. University of Colorado Department of Atmospheric Science Paper 457, 109 pp. [Available online at http://hdl.handle.net/10217/78813.]

Sitkowski, M., J. P. Kossin, and C. M. Rozoff, 2011: Intensity and structure changes during hurricane eyewall replacement cycles. *Mon. Wea. Rev.*, **139**, 3829–3847, doi:10.1175/MWR-D-11-00034.1.

Smith, R. K., C. W. Schmidt, and M. T. Montgomery, 2011: An investigation of rotational influences on tropical-cyclone size and intensity. *Quart. J. Roy. Meteor. Soc.*, **137**, 1841–1855, doi:10.1002/qj.862.

Sobel, A. H., and C. S. Bretherton, 2000: Modeling tropical precipitation in a single column. *J. Climate*, **13**, 4378–4392, doi:10.1175/1520-0442(2000)013<4378:MTPIAS>2.0.CO;2.

Stephens, G. L., 1990: On the relationship between water vapor over the oceans and sea surface temperature. *J. Climate*, **3**, 634–645, doi:10.1175/1520-0442(1990)003<0634:OTRBWV>2.0.CO;2.

Stewart, S., 2014: National Hurricane Center annual summary: 2012 Atlantic hurricane season. National Hurricane Center Tropical Cyclone Rep., 11 pp. [Available online at http://www.nhc.noaa.gov/data/tcr/summary_atlc_2012.pdf.]

Stiles, B. W., R. E. Danielson, W. L. Poulsen, M. J. Brennan, S. Hristova-Veleva, T.-P. Shen, and A. G. Fore, 2014: Optimized tropical cyclone winds from QuikSCAT: A neural network approach, **52**, 7418–7434, doi:10.1109/TGRS.2014.2312333.

Tang, B., and K. Emanuel, 2010: Midlevel ventilation's constraint on tropical cyclone intensity. *J. Atmos. Sci.*, **67**, 1817–1830, doi:10.1175/2010JAS3318.1.

——, and ——, 2012: A ventilation index for tropical cyclones. *Bull. Amer. Meteor. Soc.*, **93**, 1901–1912, doi:10.1175/BAMS-D-11-00165.1.

Uhlhorn, E. W., B. W. Klotz, T. Vukicevic, P. D. Reasor, and R. F. Rogers, 2014: Observed hurricane wind speed asymmetries and relationships to motion and environmental shear. *Mon. Wea. Rev.*, **142**, 1290–1311, doi:10.1175/MWR-D-13-00249.1.

Vecchi, G. A., and B. J. Soden, 2007: Effect of remote sea surface temperature change on tropical cyclone potential intensity. *Nature*, **450**, 1066–1070, doi:10.1038/nature06423.

Wang, Y., 2009: How do outer spiral rainbands affect tropical cyclone structure and intensity? *J. Atmos. Sci.*, **66**, 1250–1273, doi:10.1175/2008JAS2737.1.

Weatherford, C., and W. Gray, 1988: Typhoon structure as revealed by aircraft reconnaissance. Part I: Data analysis and climatology. *Mon. Wea. Rev.*, **116**, 1032–1043, doi:10.1175/1520-0493(1988)116<1032:TSARBA>2.0.CO;2.

Zhai, A. R., and J. H. Jiang, 2014: Dependence of U.S. hurricane economic loss on maximum wind speed and storm size. *Environ. Res. Lett.*, **9**, 064019, doi:10.1088/1748-9326/9/6/064019.

Zhou, W., I. M. Held, and S. T. Garner, 2014: Parameter study of tropical cyclones in rotating radiative–convective equilibrium with column physics and resolution of a 25-km GCM. *J. Atmos. Sci.*, **71**, 1058–1069, doi:10.1175/JAS-D-13-0190.1.